Collimator Design for Improved Spatial Resolution in SPECT and Planar Scintigraphy

Shahrokh Kimiaei, Stig A. Larsson and Hans Jacobsson

Departments of Hospital Physics and Diagnostic Radiology, Karolinska Hospital, Stockholm, Sweden

This paper evaluates the design of a new planar-concave collimator with nonuniform response that better matches the body shape than conventional collimators. **Methods:** The collimator properties are evaluated and assessed by means of both a simulation program and an experimental test using a prototype planar-concave collimator. **Results:** The results, for points located 150 mm from the axis of rotation, demonstrate that the ratio of radial and tangential spatial resolution in SPECT with the new collimator decreased by 40%, as compared to SPECT with a standard collimator. In planar scintigraphy, the spatial resolution improved correspondingly from 10.9 mm (FWHM) to 7.8 mm in lateral areas of the body. **Conclusion:** The new collimator reduces nonisotropic blurring in SPECT in addition to improving spatial resolution in both planar scintigraphy and in SPECT.

Key Words: planar-concave collimator; planar collimator; nonisotropic spatial resolution; parallel-hole collimators

Current collimators for planar gamma cameras are generally designed as planar grids with holes of the same size and length. The image properties of these collimators are a uniform spatial resolution and a uniform sensitivity over the entire field of view. However, a disadvantage of this conventional design is that the distance between the body surface and the collimator may vary within the field of view. In examinations of the thorax and the abdomen, for instance, optimum spatial resolution at a certain depth in the body is only achieved at the center where the body is closest to the collimator.

This inherent drawback affects both planar imaging and SPECT. In SPECT, sources at different distances from the axis of rotation will contribute to the projection data with different collimator response functions due to the varying distance between the sources and the collimator during camera rotation. This results in images where the spatial resolution varies with the distance from the center of rotation in radial and tangential directions. The latter effect, the nonisotropy of spatial resolution, produces increasingly elliptical-shaped point-spread functions with increasing distance from the center.

Various analytical methods of correction for the nonstationary spatial resolution in SPECT have been suggested and applied over the past few years. These methods have either been designed as a separate analytical correction (*1*) or a correction in combination with attenuation correction (*2,3*). Both types of methods have demonstrated that the variance in spatial resolution can be reduced. However, some of this improvement may be achieved at a cost of higher noise (*1*) or being limited to circular camera orbits and examinations of convex and uniform objects (*2,3*). Regarding the nonisotropy, improvements have been achieved essentially at the cost of degraded resolution in a

tangential direction (*2,3*) or, in some cases, a degraded overall spatial resolution (*3*).

In this paper, we present results from computer simulations and experiments of different parallel-hole collimators, aiming at a design that reduces the nonisotropic spatial resolution in SPECT. The new set of collimators, the so-called planar-concave collimators, matches the body shape in such a way that they can improve the spatial resolution in both SPECT and planar scintigraphy, as compared to conventional planar collimators.

MATERIALS AND METHODS

A SPECT Collimator Simulation Program

A collimator simulation program was developed (C2SIM) to investigate and analyze the factors responsible for nonstationary blurring in SPECT. The two-dimensional detection geometry applied for the simulations was first assessed by creating collimator files, made up as cross-sections of the desired geometry, and a set of a variables characterizing the properties of each collimator.

These collimator geometry files were used as input data to the main program, C2SIM. This program operates by projecting photons from a single point of radioactivity at (x_0, y_0) in an arbitrary object along a ray to a collimated detector at a position r on the projection axis (Fig. 1). The r, s coordinates, representing the detection plane, rotate in a fixed x, y coordinate system. The transformation of coordinates from the rotating r, s system to the fixed x, y system is performed by:

$$x = s \cos \phi - r \sin \phi$$

$$y = s \sin \phi + r \cos \phi$$

where ϕ is the angle of projection of the object.

Photons from the radioactivity located at (x_0, y_0) are assumed to be registered at the detector as projection data $p(r, \phi, \theta)$. Here, r represents the point of photon interaction in the detector along the projection axis. $|\theta| < \theta_{max}$ is the angle of oblique photon incidence to the collimator and θ_{max} is the maximum angle of oblique photon acceptance for the actual collimator. The projection data $p(r, \phi, \theta)$, obtained from the activity $\rho(x, y)$ at an incident angle θ along the projection axis r at ϕ may thus be expressed:

$$p(r, \phi, \theta) = k\rho[s_0 \cos \phi - (r - \tau) \sin \phi, s_0 \sin \phi$$
$$+ (r - \tau) \cos \phi]A(r, \phi, \theta) \, d\theta$$

where k represents the detector efficiency and the number of emitted photons per unit of activity. The factor $\tau = (AOR - s_0) \tan \theta$ is the projected distance between the orthogonal entrance and the oblique entrance of photons into the detector along the projection axis (r, θ). AOR is the distance from the axis of rotation to the detector surface. The attenuation of photons along the ray through the object and the collimator septum walls is represented by A (r, ϕ, θ) which may be described as:
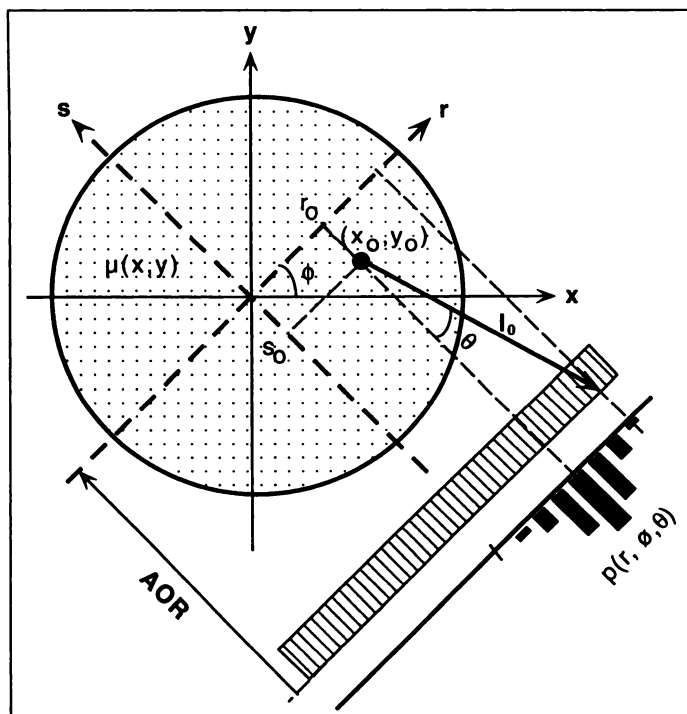
FIGURE 1. The C2SIM collimator-detection geometry.

$$A(r, \phi, \theta) = \exp\left[- \int_0^{l_0} \mu((s_0 - \xi \cos \theta) \cos \phi - (r_0 + \xi \sin \theta) \right.$$

$$\left. \times \sin \phi, (s_0 - \xi \cos \theta) \sin \phi - (r_0 + \xi \sin \theta) \cos \phi) \, d\xi \right]$$

where $l_0 = (AOR + s_0)/\cos \theta$ is the length of the oblique ray from a point (x_0, y_0) to the projection axis. The linear attenuation coefficient is $\mu(x, y)$ at a point (x, y) in the detection geometry (including the phantom and collimator septa) and $\xi(0 \le \xi \le l_0)$ is a dummy integration variable.

After the first simulation of projection data from the object to the detector at an angle ϕ, the r, s coordinate system is rotated stepwise in an angular increment $d\phi$, $(2\pi/128)$ and new projection data are computed until 128 projections are achieved over the whole angular interval of 360°. Penetration of photons through the collimator (lead) was taken into account in all simulations as well as attenuation of photons in its surrounding media. No consideration was taken to scattering of photons. All projections were finally convolved with a Gaussian distribution function with 4-mm FWHM to include the effect of intrinsic spatial resolution of the detector itself.

After generating a complete set of 128 equidistant angular projections p(r, ϕ, θ), reconstruction of a transverse section image was performed using a conventional filtered back-projection technique with a ramp filter. The geometry file was a 512×512 matrix where each matrix corresponded to 0.23 mm. The projected data were first assembled in a 1024 matrix and later converted to a 128 matrix after convolution with the Gaussian function.

SPECT Simulations

SPECT simulations were performed of a virtual 140-mm diameter cylindrical air equivalent phantom with four point sources using different collimator geometry. The sources were radially positioned at 0, 45, 90 and 135 mm from the center of the phantom. The central axis of the phantom was set aligned with the axis of rotation and the selected radius of rotation was 145 mm in all simulations. The first stimulated collimator was a conventional
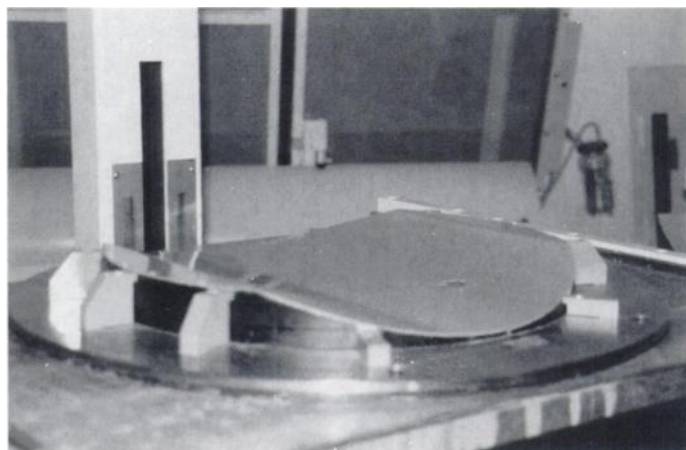

FIGURE 2. The prototype planar-concave collimator.

parallel-hole collimator (C1) with a hole diameter of 2.52 mm, a lead septum thickness of 0.23 mm and a hole length of 40.0 mm. The second (C2) and the third (C3) collimator were planar-concave collimators with their hole length increasing from 40.0 mm at the center to 80.0 mm and 120 mm, respectively, and 235 mm from the center of the collimator. All other parameters of the curved collimator were assumed to be the same as those of the conventional collimator design.

The Design of a Prototype Collimator

Based on the results obtained from the computer simulations, we manufactured a planar-concave collimator with increasing hole length in the direction perpendicular to the axis of rotation. The collimator was made up by stacking two identical 400-mm diameter circular-casted standard LEGP collimators on top of each other. The holes of these two collimators were 40 mm long with a diameter of 3.0 mm and a septum thickness of 0.33 mm. The center part of one of these two collimators was milled out to give a curvature corresponding to a cylinder of 806-mm diameter centered at 363 mm from the collimator face. Figure 2 shows an image of the prototype planar-concave collimator.

Experimental Studies: SPECT

To evaluate and compare the properties of the new collimator with those of a conventional collimator of the same kind, a 50-mm thick elliptical phantom of polystyrene was manufactured with a long axis of 320 mm and a short-axis of 240 mm. Circular holes, 5 mm in diameter were drilled at 0, 5, 10, 12.5 and 15 cm from the center along a radius long axis. A plastic tube was filled with a mixture of water and $^{99m}TcO_4^-$ to a concentration of 50 MBq/ml. This tube was mounted within one of the phantom holes at each SPECT acquisition.

A standard LEGP collimator was fitted on one camera head and the new collimator on the opposed head of a dual-head camera system. Since both circular collimators were too small to cover the entire field of view, a 5-mm thick lead plate was mounted over the unshielded areas of the field of view of each detector head. SPECT data acquisition of 360° was performed simultaneously using both detector heads.

Data acquisition and image reconstruction were performed with a matrix size of 256×256 and a pixel size of 1.65×1.65 mm^2. The radius of camera rotation was 23 cm and a 20% energy discrimination window was centered at 140 keV. Nonuniformity correction was performed separately for the two heads using flood-source images from ^{99m}Tc with 60×10^6 registered events. Image reconstruction was performed separately for the two heads with a ramp filter and a prefiltering of projected views with a two-dimensional Hamming filter (cut-off frequency $f_c = 1.2$ cm^{-1}) using the Trionix software.

Experimental Studies: Planar Scintigraphy

The difference in spatial resolution between the new planar-concave collimator and the conventional collimator for planar scintigraphy was also tested experimentally by means of phantom studies. For this purpose, five 5-mm diameter holes, were drilled at a depth of 10 mm beneath the curved edge of the elliptical polystyrene phantom. The same tubes with activity as in the previous experiment were positioned in one hole at the time where planar images were acquired using each of the collimators. The distance between the collimator and the phantom was kept as small as possible in order to obtain optimal image quality.

To illustrate the presumed clinical advantages of the new collimator for planar imaging, a bone-scan was first performed with the conventional LEGP collimator and subsequently with the new collimator mounted on a single-head gamma camera. The patient was an 85-yr-old man who underwent bone scintigraphy because of pain in the pelvis from an unknown primary malignancy. All procedures for the examinations were the same as those used in daily routine with administration of 500 MBq ^{99m}Tc-HDP and an acquisition time of 10 min/view.

RESULTS

SPECT Simulations

The spatial resolution achieved by simulating and reconstructing SPECT data of point sources located at various depths are presented in Figures 3A and B. These figures show the spatial resolution, expressed as tangential FWHM ($FWHM_t$), radial ($FWHM_r$) and their ratios for each of the three simulated types of collimators. As demonstrated by Figure 3A, the tangential spatial resolution in SPECT decreases almost equally with increasing distance from center for all three collimators. The spatial resolution in radial direction, on the other hand, remains almost constant for the planar collimator (C1) while decreasing for the two planar-concave collimators (C2 and C3). The improved spatial resolution with increasing distance from the center in both tangential and radial directions, results in a tangential/radial ratio that is closer to unity for the latter two collimators than for the conventional one and, hence, to a reduced nonisotropic image blur.

Experimental Studies: SPECT

Figure 4A and B and Figure 5 show the superimposed point source images obtained after reconstruction with each of the collimators and the ratios of the tangential and the radial FWHM for the point source at each location and for each collimator type. It can be seen from Figure 5 that the tangential to radial ratio is decreased from 0.73 to 0.52 or 40%, due to improved radial spatial resolution and, therefore, the ability of differing point sources located laterally is increased.

Experimental Studies: Planar Scintigraphy

The FWHM values obtained with the activity tube positioned in the holes along the long axis of the elliptical polystyrene phantom and in the corresponding holes 10 mm below the front surface are shown in Figure 6 as a function of their distance from the center. While FWHM remains constant for sources along the long axis of the elliptical phantom for the standard collimator, it improves with increasing distance from the center for the planar-concave collimator due to its increasing hole length. On the other hand, FWHM for the standard collimator is considerably impaired, as compared to that of the planar-concave collimator, for sources located along a curved line at a 10-mm depth from the elliptical phantom surface.

An example of the clinical usefulness of these properties, related to the planar-concave collimator, is presented in Figure 7. This figure shows a frontal view of the skeletal uptake in the
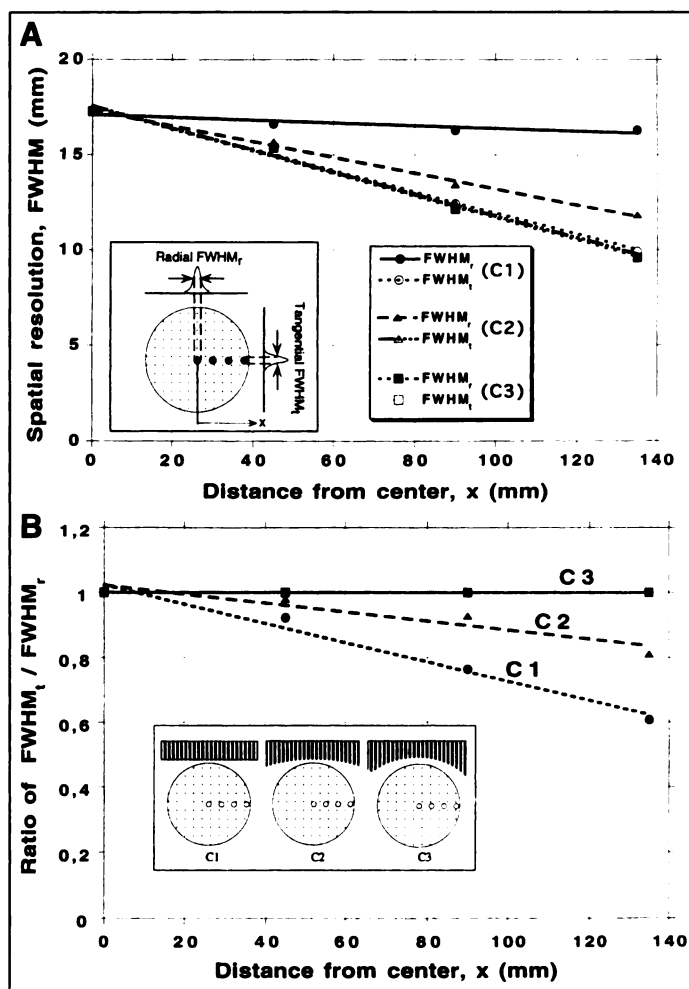

FIGURE 3. Spatial resolution, assessed by simulated SPECT data with three different collimator designs. (A) FWHM in tangential and radial directions as a function of source distance from the center, x. (B) The ratios of tangential and radial spatial resolution and a schematic drawing of the collimator types.

thoracic region of a patient, 3 hr after administration of ^{99m}Tc-HDP and using both a standard and our prototype planar-concave collimator. Activity profiles along a line passing through sternum and the observed metastasis are also
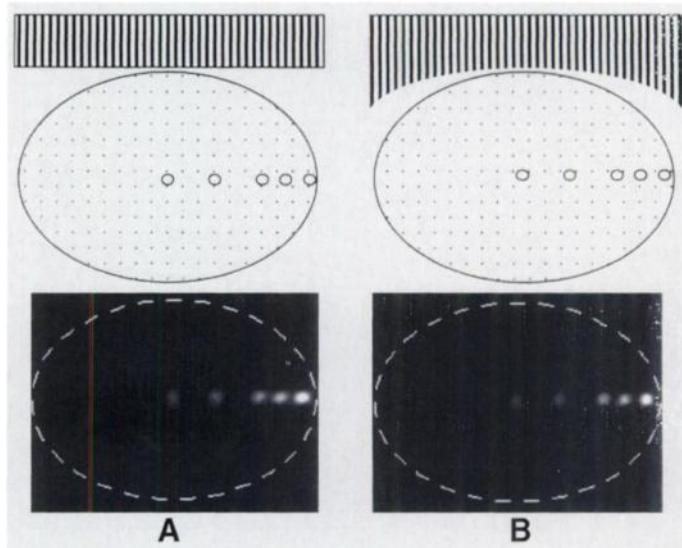

FIGURE 4. Experimentally-obtained SPECT images of five line sources in an elliptical polystyrene phantom using (A) the conventional parallel-hole collimator and, (B) the planar-concave prototype collimator.
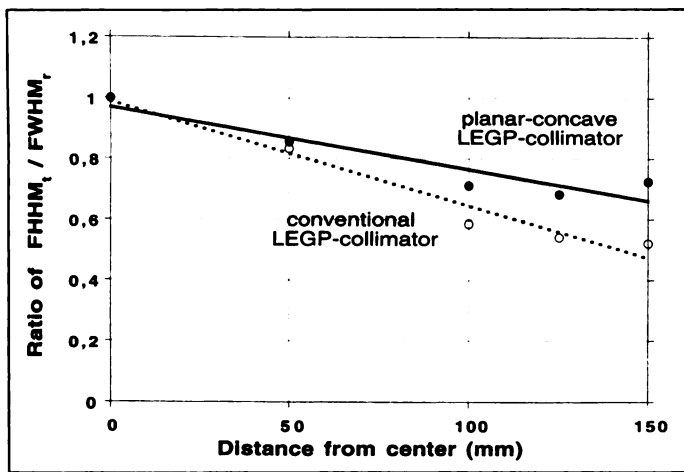
FIGURE 5. Ratio of spatial resolution in tangential (FWHM$_t$) and in radial direction (FWHM$_r$), as a function of distance, x from the center. Data obtained from the sources, illustrated in Figure 4.

shown. Since the spatial resolutions of both collimators are almost equal at the center of the field of view, the uptake in the sternum may be used as a reference for evaluating the peripheral imaging quality.

Using the sternum uptake (at the center of each collimator) as a reference area, these profiles show that the contrast, or the uptake ratio of the metastasis and the sternum, is increased when imaging with the planar-concave collimator. The metastasis/sternum ratio is 1.16 using the conventional collimator while it is 1.46 using the new collimator. The higher relative uptake ratio is due to the improved spatial resolution in lateral areas of the new collimator.

Due to the improved image sharpness in these regions, higher detectability of suspected findings may be achieved clinically with this type of collimator. However, this should be investigated further when an optimally-designed version of the prototype collimator is available.

DISCUSSION

We have presented the design and evaluation of a planar-concave collimator for application in both SPECT and planar gamma camera scintigraphy. Results obtained from both simulations and measurements show that planar-concave collimators produce a better lateral spatial resolution than comparable
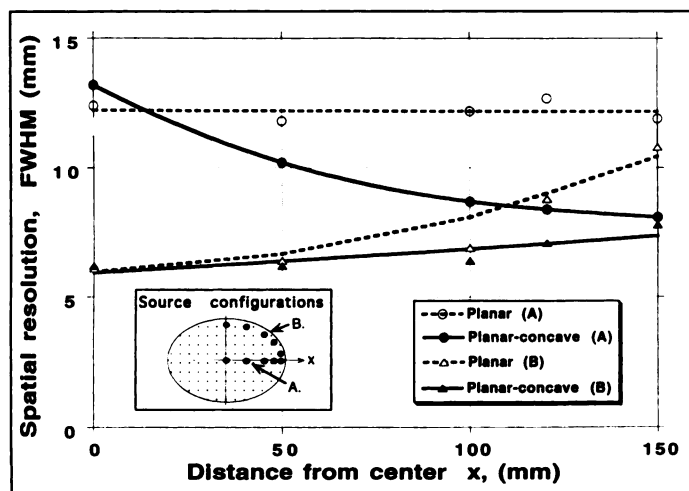

FIGURE 6. Spatial resolution (FWHM) in planar scintigraphy with the conventional planar- and the planar-concave prototype collimator. (A) Represents positions along the long-axis and (B) positions at 10-mm depth from elliptical phantom surface.
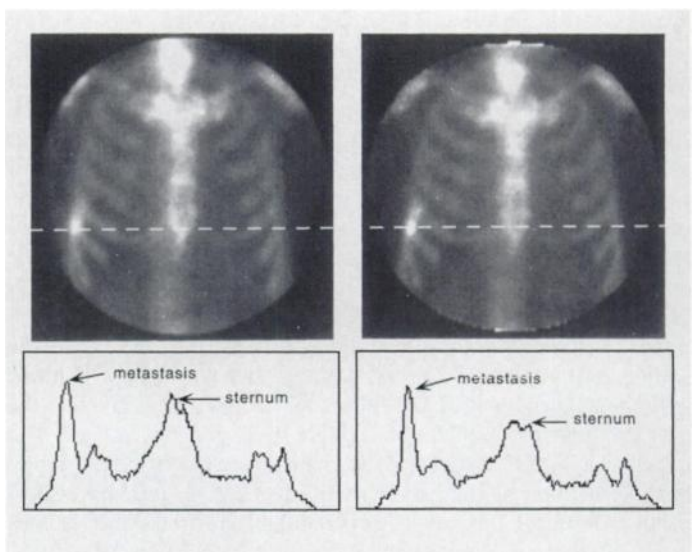

FIGURE 7. Bone scan of the thoracic region of a patient with a malignancy in the lateral part of a right rib, obtained by using (A) the planar collimator and (B) the planar-concave prototype collimator.

conventional collimators. All simulations were made from nonattenuation corrected images in order to avoid any influence from incomplete attenuation correction routines.

With such a collimator, one achieves a more uniform spatial resolution (FWHM) at a fixed depth from the surface of elliptical body regions compared to that of a conventional planar collimator. With the prototype collimator used, the spatial resolution at a 10-mm depth in the phantom, varied only from 6 mm to 7.5 mm (25%) from the center to the edge of an elliptical phantom. Using a conventional planar collimator, the spatial resolution varied correspondingly from 6 to 11 mm, or 83%.

This type of collimator design also improves the spatial resolution in SPECT. It does not remove the nonstationary blurring caused by the collimator, but it reduces the nonisotropic distortion in SPECT. The nonisotropy with the prototype collimator, as assessed by the ratio of spatial resolution in radial and tangential directions, was reduced by 40% for sources located 150 mm away from center of rotation as compared to a conventional parallel-hole collimator.

A drawback of the new collimator design is that the sensitivity varies over the field of view. For our prototype collimator the sensitivity varied by a factor of two from the center towards its edges, 160 mm away. Thus, a sensitivity compensation has to be performed, for instance, by means of a flood-source correction. Since the sensitivity varies only smoothly, it is not likely that there should be any more high-frequency sensitivity components at the center where the largest artifact amplitudes may appear (4,5). Furthermore, the laterally-reduced sensitivity may contribute to a lower signal-to-noise ratio for extended sources. On the other hand, the lower sensitivity at the edges is partly counterbalanced in SPECT by the lower signal at the center due to the photon attenuation. The impact on noise due to a nonuniform sensitivity over the field of view has not yet been fully analyzed. Further investigations are needed in order to assess this effect on reconstructed SPECT images.

The experimental results of this work were obtained with a prototype collimator. This collimator was made with a pair of old and slightly defective cast collimators which were not purchased at the same time. Even though the matching of the hole pattern was quite good when stacking the two together, a perfect matching was never achieved. Finally, the curvature

and, thus, the spatial resolution characteristics had to be selected on the basis of the available collimators.

By manufacturing a new optimal planar-concave collimator, it may be possible to remove most of the present nonisotropic blurring in SPECT. It should also be possible to design a collimator with curvature that better matches the thoracic and the abdominal regions of the body.

ACKNOWLEDGMENTS

REFERENCES

1. Lewitt RM, Edholm PR, Xia W. Fourier method for correction of depth-dependent collimator blurring. *SPIE* 1989;1092:232–239.
2. Soares EJ, Bryne CL, Glick SJ, et al. Implementation and evaluation of an analytical solution to the photon attenuation and nonstationary resolution problem in SPECT. *IEEE Trans Nucl Sci* 1993;40:1231–1237.
3. Elmbt L, Walrand S. Simultaneous correction of attenuation and distance-dependent resolution in SPECT: an analytical approach. *Phys Med Biol* 1993;38:1207–1217.
4. Larsson SA. Gamma camera emission tomography: development and properties of a multi-sectional emission computed tomography system. *Acta Radiol* 1980(suppl);363:1–80.
5. Axelsson B, Israelsson A, Larsson S. Nonuniformity-induced artifacts in SPECT. *Acta Radiol (oncol)* 1983;22:215–224.

Comparative Methods for Quantifying Thyroid Volume Using Planar Imaging and SPECT

Habib Zaidi

Department of Radiation Physics, Malmö General Hospital, Malmö, Sweden

SPECT enables improved accuracy over planar imaging in the determination of the volume since it is derived from three-dimensional data rather than from a two-dimensional projection with a certain geometric assumption regarding the thyroid configuration. **Methods:** By using the phantoms of known volume, it was possible to estimate the accuracy of three different methods of determining thyroid volume from planar imaging used in clinical routine: the standard method used at Malmö General Hospital; a modified version of this standard method; and the method used in Lund Hospital in combination with different ways of defining the regions of interest (ROIs), and to assess the accuracy of the adaptive threshold or gray level histogram method based on SPECT imaging which determines a threshold that maximizes the separability of two classes (object and surround). **Results:** The correlation coefficient (r) and the regression equation between the true (x) and the calculated volume (y) were as follows: $r = 0.99$ and $y = 0.98x + 3.6$ using SPECT and the gray level histogram method for edge detection combined with attenuation and scatter corrections, while $r = .97$ and $y = 0.67x + 3.2$ using the standard method based on planar scintigraphy. The standard method as used in routine was found to produce large errors (24.8%). The error on the volume estimate was reduced to ~7% for volumes in the range 16-to-75 ml using SPECT. **Conclusion:** Compared with conventional scintigraphy, thyroid phantom volumes were most accurately determined with SPECT when attenuation and scatter corrections are performed, which allows accurate radiation dosimetry in humans without the need for assumptions on organ size or concentration.

Key Words: planar imaging; SPECT; volume estimation; thyroid

J Nucl Med 1996; 37:1421–1426

The weight of the thyroid gland is an important factor entering into the determination of the activity of ^{131}I to be administered for the treatment of hyperthyroidism caused by Graves' disease (*1*). There is nearly 50 years of experience in the use of ^{131}I for the management of patients both with hyperthyroidism and thyroid cancer (*2*). As a result of this experience radioiodine therapy is now considered to be the treatment of choice, offering many advantages over surgery. There are still, however, controversies regarding the role and management of radioiodine therapy in the treatment of thyrotoxicosis. These controversies are due mainly to the difficulties in determining accurately the mass of the thyroid gland and hence the radiation dose delivered (*3*).

Scintigraphy of the thyroid gland is usually carried out taking a single frontal image. The volume of the gland is then calculated using an empirical formula for the correlation between the cross-sectional area of the gland in the frontal image and the volume. Thyroid volume can be indirectly determined from the anterior and lateral views of radionuclide images, but with a certain geometric assumption regarding the thyroid configuration. The obvious difficulty, however, of matching a geometric form to such a complex three-dimensional organ made it necessary to further develop the technique. Several formulas have been proposed (*4,5*) but these methods have been shown to produce large inherent inaccuracy. Rotating scintillation camera SPECT systems are ideal for such volumetric quantification because they are true three-dimensional volume imaging systems. The advantage of the ECT approach is its complete independence of thyroid shape, since no geometric assumption is necessary.

The work presented in this article was designed to study the errors induced by thyroid volume determination using different calculation methods based on planar imaging routinely being used at both the Malmö and Lund University Hospitals.

MATERIALS AND METHODS

Phantom Studies

The first step was to produce thyroid phantoms of different shapes and sizes. For this purpose, plastic ellipsoids and a MIRD thyroid phantom were constructed. Their volumes were carefully determined by weight after the phantoms were filled with water. The experimental MIRD thyroid phantom was designed to repre-